Event-triggered feedback in noise-driven phase oscillators

Justus A. Kromer,[1,*] Benjamin Lindner,[1,2] and Lutz Schimansky-Geier[1,2]
[1]*Department of Physics, Humboldt-Universität zu Berlin, Newtonstrasse 15, 12489 Berlin, Germany*
[2]*Bernstein Center for Computational Neuroscience Berlin, Berlin, Germany*
(Received 5 November 2013; published 31 March 2014)

Using a stochastic nonlinear phase oscillator model, we study the effect of event-triggered feedback on the statistics of interevent intervals. Events are associated with the entering of a new cycle. The feedback is modeled by an instantaneous increase (positive feedback) or decrease (negative feedback) of the oscillator frequency whenever an event occurs followed by an exponential decay on a slow time scale. In addition to the known excitable and oscillatory regimes, which are separated by a saddle node on invariant circle bifurcation, positive feedback can lead to bistable dynamics and a change of the system's excitability. The feedback has also a strong effect on noise-induced phenomena like coherence resonance or anticoherence resonance. Both positive and negative feedback can lead to more regular output for particular noise strengths. Finally, we investigate serial correlations in the sequence of interevent intervals that occur due to the additional slow dynamics. We derive approximations for the serial correlation coefficient and show that positive feedback results in extended positive interval correlations, whereas negative feedback yields short-ranging negative correlations. Investigating the interplay of feedback and the nonlinear phase dynamics close to the bifurcation, we find that correlations are most pronounced for optimal feedback strengths.

DOI: 10.1103/PhysRevE.89.032138 PACS number(s): 05.40.−a, 05.10.Gg

I. INTRODUCTION

Self-sustained oscillations occur in many physical, chemical, or biological systems [1]. If variations of the amplitude are negligible, a widely used model in this context is the well-known dynamics for the phase ϕ [2]:

$$\dot{\phi}(t) = \omega_0 - \epsilon \sin[\phi(t)]. \tag{1}$$

Here ω_0 represents the oscillator frequency in the case $\epsilon \to 0$. Without loss of generality, we restrict our investigations on $\omega_0 > 0$. By rescaling ω_0 and the time scale, ϵ can be set to one (dimensionless units). The system can show both excitable ($0 < \omega_0 < 1$) and oscillatory ($\omega_0 > 1$) dynamics. Both regimes are separated by a saddle node on invariant circle (SNIC) bifurcation at $\omega_0 = 1$, which makes the system a good model for class I excitability [3]. Equation (1) is known as the Adler's equation [4] and is often used to describe excitability in optical systems [5,6] or in neuroscience [7] and particle motion in a tilted periodic potential or to study the onset of resistance in superconducting Josephson junctions [8,9]. Generally, such oscillators are studied when driven by time-dependent forces, such as noise, when subjected to time delayed feedback [10] or when they are coupled in networks.

For many applications, particular events in the phase dynamics are of foremost interest, e.g., the crossings of a threshold value $\phi = 2\pi$ as associated with, for instance, the generation of an action potential in a nerve cell, the dropout of light intensity in an excitable laser, the release of a messenger by a cell, or the division of a cell. The statistics of the intervals between these events Δt (interevent intervals, or, in the following, IEI) in the presence of noise have been studied intensely in the neurobiological context for the related class of integrate-and-fire (IF) models [11,12] (here IEIs are referred to as interspike intervals).

In some systems, the events directly influence the dynamics of the oscillator. Put differently, in these systems we find event-triggered feedback mechanisms. Generally, the oscillator's dynamics becomes more interesting if such feedback mechanisms are taken into account. For neurons, negative feedback can arise from slow inhibitory ionic currents that change over several IEIs. This can lead to spike-frequency adaptation [13,14], noise shaping [15], and interval correlations [16,17]. Feedback, however, can be also positive, for instance, due to variations in the external potassium concentration, which are triggered by neural spiking [18,19] and act on a time scale which is large compared to the individual IEIs [20]. In some systems strong positive feedback can change the dynamics fundamentally, leading, for instance, to bursting behavior [21]. In laser physics positive feedback for particular modes can be used to self-mode-lock lasers [22] and it seems to be a plausible explanation of positive IEI correlations, reported in Ref. [23]. In cell biology, positive feedback loops occur, for instance, in the lactose utilization network of *Escherichia coli*, where the production of lactose permease increases its expression level and is assumed to be a reason for bistability in the lactose utilization [24,25]. However, the effect of positive feedback, especially in the presence of noise, is so far only poorly understood.

Analytical attempts to deal with an additional feedback dynamics in a pulse generator were mainly limited to approximations of the firing rate [13,26] and weak-feedback approximations for the IEI statistics of a very simple IF model, the so-called perfect IF model [27]. Regarding the more striking feature of the feedback-induced interspike interval correlations, approximations until recently were carried out for the perfect IF model [16], variants that deviate only by a weak nonlinearity from it [28] or IF models subjected to a weak feedback [29]. In Ref. [30], a general theory has been worked out to calculate patterns of interval correlations in multidimensional IF models. All these studies focused on a

*justuskr@physik.hu-berlin.de

negative feedback, however, and did not address the generic phase oscillator dynamics [Eq. (1)].

Here we study the dynamics of a phase oscillator in the vicinity of a SNIC bifurcation from the excitable to the oscillatory regime, which is subject to noise and an event-triggered feedback. We consider feedback strengths that can attain both positive and negative values and derive analytic approximation for several statistical measures by considering a large time scale separation between the phase and the feedback dynamics.

Our results for negative feedback are in line with previous studies: We find suppression of low-frequency power in the power spectrum of the spike train [31,32] and negative serial correlations in the series of N subsequent IEIs $\Delta t_1, \ldots, \Delta t_N$ [13,33–35]. More remarkably, we find that positive feedback causes a number of effects. In the deterministic system, bistability emerges in the form of the coexistence of a stable node (SN) and a limit cycle (LC) attractor. Second, we study the effect of noise and feedback on the system. Here we focus on the excitable and the oscillatory regime. We find anticoherence resonance in the excitable regime—IEI variability is maximized at a finite noise intensity—and observe positive IEI correlations in both the excitable and the oscillatory regimes. Interestingly, IEI correlations for both positive and negative feedback behave nonmonotonically with the feedback strength, if the system is close to the bifurcation.

Our paper is organized as follows. In Sec. II we introduce the model and the statistics of interest. We study first, in Sec. III, the nonlinear dynamics of the system without noise (including a bifurcation analysis) and explore the effects of noise and feedback on the mean frequency of the oscillator. In Sec. IV, we investigate the IEI variability and the power spectrum of the phase oscillator with feedback. Section V is devoted to IEI correlations. Finally, we conclude by summarizing our results and discussing their broader implications. All details concerning simulation techniques and analytical calculations of the serial correlation coefficient are given in Appendixes A and C, respectively.

II. THE MODEL

In order to implement the feedback we define an event to occur whenever the phase reaches the threshold 2π, i.e., $\phi(t_i) = 2\pi$, where t_i denotes the time of the ith event. Afterwards, the phase is reset ($\phi \to 0$). The feedback acts on the phase oscillator by increasing (positive feedback) or reducing (negative feedback) its frequency. Thus, we add a time-dependent part $\Delta\omega(t)$ to the frequency ω_0, which accounts for the frequency adaptation due to the feedback. Consequently, Eq. (1) becomes

$$\dot{\phi}(t) = \Delta\omega(t) + \omega_0 - \sin[\phi(t)] + \sqrt{2D}\xi(t). \tag{2}$$

Combined with the reset condition,

$$\text{if} \quad \phi = 2\pi, \quad \text{then} \quad \phi \to 0. \tag{3}$$

Here we also added white Gaussian noise [$\langle\xi(t)\rangle = 0$ and $\langle\xi(t)\xi(t')\rangle = \delta(t-t')$] with a noise strength D, where $\langle\cdot\rangle$ denotes averaging.

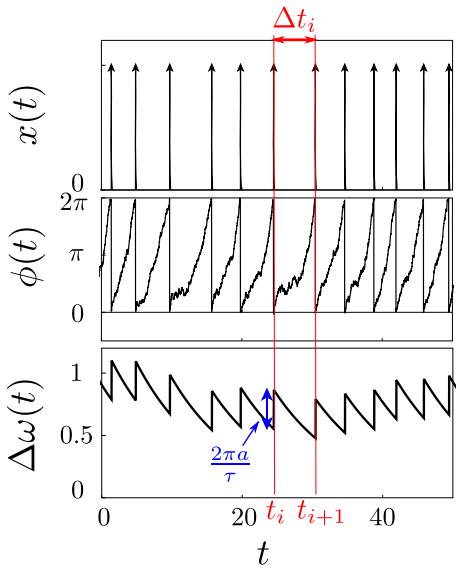

FIG. 1. (Color online) Time evolution of $x(t)$, $\phi(t)$, and $\Delta\omega(t)$ (from top to bottom) for $\omega_0 = 1.1$, $a = 0.5$, $\tau = 10$, and $D = 0.1$.

When an event occurs, the system perceives a kick which changes $\Delta\omega$. This is modeled by the additional dynamics

$$\tau \frac{d}{dt}\Delta\omega(t) = -\Delta\omega(t) + 2\pi a\, x(t), \tag{4}$$

where

$$x(t) = \sum_i \delta(t - t_i) \tag{5}$$

is the sequence of kicks at the event times t_i.

Equation (4) describes the dynamics of $\Delta\omega$, evolving on the feedback time scale τ. Due to the first term, it decays towards zero from any deviation. The second term models the feedback and alters $\Delta\omega$ by an amount of $2\pi a/\tau$ whenever an event occurs ($t = t_i$). This is illustrated in Fig. 1 for a positive feedback strength $a > 0$, showing the time evolution, and in Fig. 2 (center), illustrating the trajectory in the $(\phi, \Delta\omega)$ space. Thus, a cycle consists first of a part where ϕ and $\Delta\omega$ evolve according to the Eqs. (2) and (4), respectively. Second, if ϕ reaches the threshold, the reset condition Eq. (3) is applied. Finally, in the third step, $\Delta\omega$ is altered by an amount of $2\pi a/\tau$. Note that putting $a = 0$ yields in the stationary case always the situation without feedback.

After some transient behavior, the rate becomes stationary and we define the oscillator's mean firing rate, which describes the average rate at which events occur,

$$r = \frac{\langle\dot{\phi}(t)\rangle}{2\pi} = \langle x(t)\rangle = \frac{1}{\langle\Delta t_i\rangle}. \tag{6}$$

Here the average is taken over a time interval large compared to the individual IEIs $\Delta t_i = t_{i+1} - t_i$, i.e., the time the oscillator needs to reach $\phi = 2\pi$ when started at $\phi = 0$.

By averaging Eq. (4), we obtain

$$\tau\left\langle\frac{d}{dt}\Delta\omega\right\rangle = -\langle\Delta\omega\rangle + 2\pi a\langle x(t)\rangle. \tag{7}$$

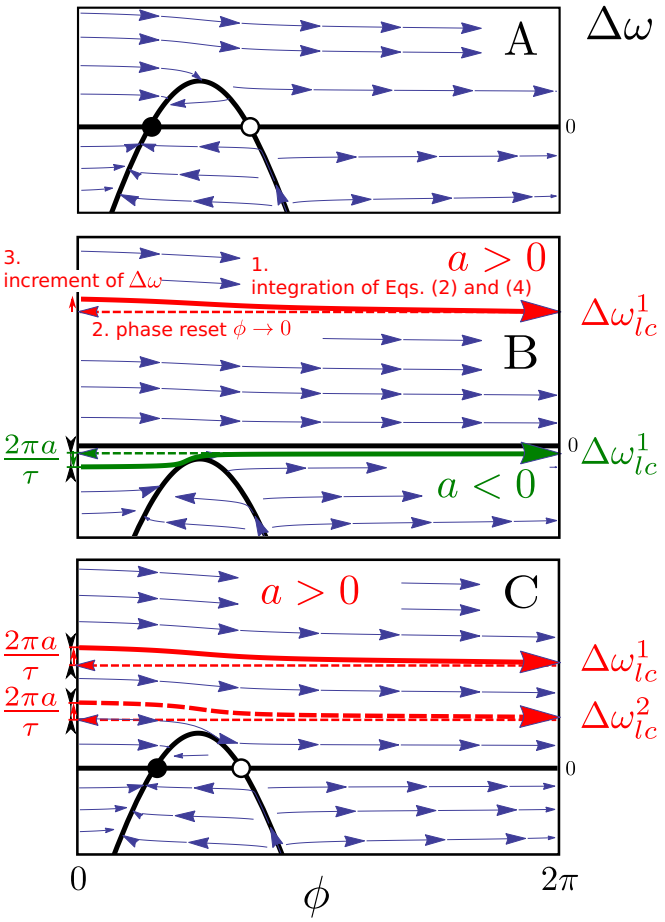

FIG. 2. (Color online) Fixed points and trajectories (colored lines) on stable (bold lines) and unstable (thick dashed line) LCs in the phase space for the excitable regime (A), the oscillatory regime (B), and the bistable regime (C) for $D = 0$ (see Fig. 4). Stable nodes (black circles), saddles (white circles), and the velocity field (small arrows) are depicted. The nullclines for the Eqs. (2) and (4) are marked by black lines. Labels ($a > 0$) and ($a < 0$) indicate LCs for positive and negative feedback, respectively. Arrows on LCs illustrate the corresponding directions. Trajectories reach the corresponding value of $\Delta\omega_{lc}$ at $\phi = 2\pi$ and start with an offset of $2\pi a/\tau$ to $\Delta\omega$ after the reset. Here $\Delta\omega_{lc}^i := \Delta\omega_{lc}(\Delta t_{\rm det}^{(i)})$ according to Eqs. (14) and (17). Parameters: (A) $\omega_0 = 0.8, \tau = 50$; (B) $\omega_0 = 1.05, \tau = 50, a = \pm 0.5$; (C) $\omega_0 = 0.85, \tau = 50, a = 0.55$.

In the stationary case, the left-hand side should be zero and we obtain

$$\langle \Delta\omega \rangle = 2\pi a r. \tag{8}$$

Using Eq. (8) in the averaged Eq. (2) yields

$$r = \frac{\omega_0 - \langle \sin[\phi(t)] \rangle}{2\pi(1-a)}. \tag{9}$$

Note that $\phi(t)$ is the solution of Eq. (2) in the presence of feedback.

Interestingly, the limit of $a \nearrow 1$ leads to infinite r if $\omega_0 > 1$. In this case the unknown numerator is positive, since $\langle \sin[\phi(t)] \rangle \leqslant 1$. Here $\nearrow$ denotes the left-hand limit. For such strong positive feedback, the deterministic decay of $\Delta\omega$ cannot balance the increase of $\Delta\omega$ due to the kicks after each event and the assumption of stationarity $\langle \Delta\dot{\omega} \rangle = 0$ does not hold. To study the stationary regime, we therefore concentrate on $a < 1$.

III. MEAN INTEREVENT INTERVAL

A. Deterministic case

At first, we concentrate on the deterministic case ($D = 0$). Here, after some transient behavior, all IEIs become equal $\Delta t_i = \Delta t_{\rm det}$ for all i. If no feedback is applied, $\Delta\omega$ will converge to zero and the IEIs can be calculated by integrating Eq. (2), which yields [36]

$$\Delta t_{\rm det,0} = \frac{2\pi}{\sqrt{\omega_0^2 - 1}}. \tag{10}$$

Here the index 0 marks the nonfeedback solution for the mean IEI. Note that positive real solutions for $\Delta t_{\rm det,0}$ exist only in the oscillatory regime $|\omega_0| > 1$.

If, however, feedback is applied ($a \neq 0$), the dynamics becomes more complex. Here the deterministic behavior can be understood by evaluating the time-dependent frequency adaptation $\Delta\omega$. Assume, that the system evolves on a LC, and let $\Delta\omega_{lc}$ be the value of $\Delta\omega$ just before an event occurs, i.e.,

$$\lim_{t \nearrow t_k} \Delta\omega(t) = \Delta\omega_{lc}. \tag{11}$$

After reset, $\Delta\omega$ changes to $\Delta\omega_{lc} + 2\pi a/\tau$, which yields the initial conditions for the next IEI. Corresponding phase portraits are illustrated in Fig. 2 (center) for positive and negative feedback, respectively. We can integrate Eq. (4) for one IEI, resulting in

$$\Delta\omega(t) = \left(\Delta\omega_{lc} + \frac{2\pi a}{\tau}\right) \exp\left(-\frac{t - t_k}{\tau}\right), \quad t_k \leqslant t < t_k + \Delta t_{\rm det}. \tag{12}$$

Since after one IEI $\Delta\omega$ reaches $\Delta\omega_{lc}$ again, i.e.,

$$\lim_{t \nearrow t_k} \Delta\omega(t) = \lim_{t \nearrow t_k + \Delta t_{\rm det}} \Delta\omega(t) = \Delta\omega_{lc}, \tag{13}$$

we obtain an explicit expression for $\Delta\omega_{lc}$:

$$\Delta\omega_{lc} = \frac{2\pi a}{\tau\left[\exp\left(\frac{\Delta t_{\rm det}}{\tau}\right) - 1\right]}. \tag{14}$$

In the following, we consider a slow feedback time scale τ, i.e., $\tau \gg \Delta t_{\rm det}$. In this case, we can expand $\Delta\omega(t)$ [Eq. (12)] in the small parameter $\Delta t_{\rm det}/\tau$. Using that $t \in [t_k, t_k + \Delta t_{\rm det}]$ and $\Delta\omega_{lc} = 2\pi a/\Delta t_{\rm det} + \mathcal{O}(\Delta t_{\rm det}/\tau)$ [see Eq. (14)], the zeroth order Taylor expansion for $\Delta\omega(t)$ reads

$$\Delta\omega(t) = \frac{2\pi a}{\Delta t_{\rm det}} + \mathcal{O}\left(\frac{\Delta t_{\rm det}}{\tau}\right). \tag{15}$$

Note that the zeroth order term equals the time-averaged frequency adaptation in Eq. (8). Using only the zeroth order in Eq. (2) for $D = 0$ leads to the solvability condition

$$\Delta t_{\rm det} = \frac{2\pi}{\sqrt{\left(\omega_0 + \frac{2\pi a}{\Delta t_{\rm det}}\right)^2 - 1}}. \tag{16}$$

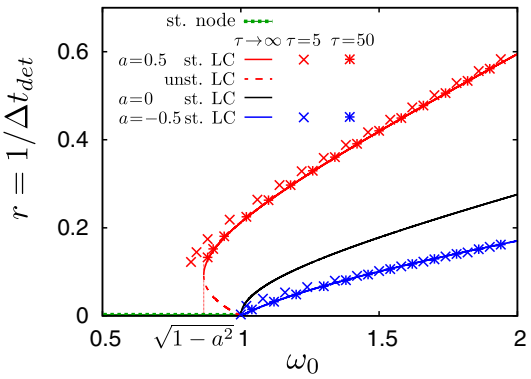

FIG. 3. (Color online) Solutions for the steady state firing rate r for $D = 0$ in the limit $\tau \to \infty$ (lines) and results from simulation (points) for $\tau = 5$ and $\tau = 50$. For positive feedback $a > 0$ (red line) two solutions of Eq. (17) exist and describe oscillations on a stable (solid line, st. LC) and an unstable (dashed line, unst. LC) LC, corresponding to the inverse $\Delta t_{\rm det}^{(1),(2)}$, respectively. The solution for $a = 0$ (black line) is given by Eq. (10). For $a < 0$ (blue line) only one solution ($\Delta t_{\rm det}^{(1)}$) exists, describing oscillations on a stable LC. Independently of a a solution $r = 0$ (green dashed line) exists for $\omega_0 < 1$.

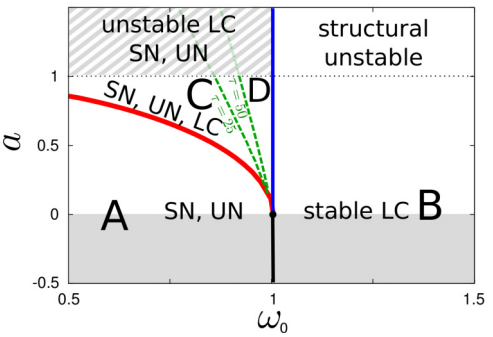

FIG. 4. (Color online) Dynamical regimes in the (ω_0,a) parameter space for $\tau \to \infty$. Capital letters name the excitable (A), the oscillatory (B), and the bistable regimes (C and D). Topological properties are denoted by SN (stable node), UN (unstable node), and LC (limit cycle). Thick lines indicate bifurcations between different regimes, dashed lines indicate bifurcations that occur for finite τ, and the dotted line separates the region where trajectories diverge.

Solving the resulting quadratic equation for $\Delta t_{\rm det}$ yields

$$\Delta t_{\rm det}^{(1),(2)} \approx \frac{2\pi}{\omega_0^2 - 1}\left[\pm\sqrt{\omega_0^2 + (a^2-1)} - a\omega_0\right], \quad \Delta t_{\rm det} \ll \tau. \tag{17}$$

By comparison with simulations, we found that positive real solutions $\Delta t_{\rm det}^{(1)}$ correspond to the cycle period of oscillations on a stable LC, whereas positive real solutions $\Delta t_{\rm det}^{(2)}$ correspond to the cycle period of oscillations evolving on an unstable LC.

In agreement with Eq. (9), the solution $\Delta t_{\rm det}^{(1)}$ runs to zero (infinite rate) for $a \nearrow 1$ when $\omega_0 \neq 1$. However, positive solutions $\Delta t_{\rm det}^{(2)}$ also exist for $a \geqslant 1$, if $\omega_0 < 1$ (dashed region in Fig. 4). They describe oscillations on an unstable LC which separates the basin of attraction of the SN from a regime where the system speeds up to infinite rate.

For $a < 1$ we find three qualitatively different regimes. Figure 3 depicts the resulting firing rates $r = 1/\Delta t_{\rm det}^{(i)}$, for $i = 1,2$, and Fig. 4 illustrates the different regimes in the (ω_0,a) parameter space. The corresponding dynamics is illustrated in Fig. 2.

(A) [Fig. 2 (top)] For $0 < a < 1$ and $\omega_0 < \sqrt{1-a^2}$ and for $a \leqslant 0$ and $\omega_0 < 1$, Eq. (17) has no real solution. Here the only stable equilibrium is the SN and only noisy excitations can lead to new events.

(B) [Fig. 2 (center)] For $a < 1$ and $\omega_0 > 1$, only $\Delta t_{\rm det}^{(1)}$ is positive. Here the system possesses a stable LC for both negative and positive feedback, respectively.

(C) [Fig. 2 (bottom)] For $0 < a < 1$ and $\sqrt{1-a^2} < \omega_0 < 1$, Eq. (17) has the two positive real solutions $\Delta t_{\rm det}^{(1)}$ and $\Delta t_{\rm det}^{(2)}$. Simulations of trajectories show that positive solutions of $\Delta t_{\rm det}^{(2)}$ correspond to slow oscillations on an unstable LC (dashed lines), which separates the basins of attraction of the stable LC, described by oscillations with period $\Delta t_{\rm det}^{(1)}$ (bold lines), and the SN (black dot). Here bistability between the SN and the stable LC occurs.

These regimes are separated by different bifurcations, indicated by thick lines in Fig. 4, which can be studied using the positions of the stable $(\phi_{st},\Delta\omega_{st}) = (\arcsin[\omega_0],0)$ and unstable node $(\phi_{ust},\Delta\omega_{ust}) = (\pi - \arcsin[\omega_0],0)$ and the linearized system of the Eqs. (2) and (4) evaluated at fixed $0 < \phi_0 < 2\pi$ and $\Delta\omega_0$,

$$\begin{pmatrix}\dot\phi\\ \dot{\Delta\omega}\end{pmatrix} = \begin{pmatrix}-\cos(\phi_0) & 1\\ 0 & -\frac{1}{\tau}\end{pmatrix}\begin{pmatrix}\phi-\phi_0\\ \Delta\omega-\Delta\omega_0\end{pmatrix}. \tag{18}$$

Using the solutions for the mean IEI [Eq. (17)], one can also study the existence of the LCs for $\tau \to \infty$. The analysis for finite τ was done by numerical simulations of trajectories.

For negative feedback (light gray region in Fig. 4) the regime A transforms into the regime B via SNIC bifurcation at $(\phi,\Delta\omega) = (\pi/2,0)$ (black line in Fig. 4). A third regime C and for finite τ a fourth regime D exist for $a > 0$. Here a stable and an unstable LC are born via saddle-node LC bifurcation at $\sqrt{1-a^2} = \omega_0$ (red line) and the two solutions of Eq. (17) coincide. The existence of LCs for finite τ was verified by simulations for $\tau = 25,50,100$. For finite τ, the unstable LC approaches the UN and, finally, vanishes via a subcritical homoclinic orbit (SHO) bifurcation [positive sum of eigenvalues of the Jacobian in Eq. (18)] (green dashed lines), if ω_0 is increased. At $\omega_0 = 1$ the two equilibria annihilate each other in a saddle-node (off cycle) bifurcation (fold) (blue line).

In the limit of large τ the SHO and fold bifurcation occur both at $\omega_0 = 1$. Here both eigenvalues of the Jacobian [Eq. (18)] become zero ($-1/\tau \to 0$), leading to a Bogdanov-Takens bifurcation. However, for finite τ the $\Delta\omega$ direction is always stable, and the bifurcation at $\omega_0 = 1$ is of fold ($a > 0$) or SNIC ($a \leqslant 0$) type.

We also find that the rate for finite τ is higher than in the limit $\tau \to \infty$ (see Fig. 3) and that the range of bistability extends to smaller values of ω_0. In the presence of positive feedback, the saddle-node bifurcation of the equilibria at

$\omega_0 = 1$ changes from on cycle (SNIC) to off cycle. This affects the system's response to a slowly increasing ω_0 and, therefore, its excitability class [7]. At $\omega_0 = 1$ the SN vanishes and events are produced. Now, the distance to the saddle-node bifurcation is increased by an amount of $2\pi a/\tau$ after each event. For small τ and large a the system leaves the vicinity of the bifurcation after the first event and produces events at a high rate even for ω_0 close to one. This leads to class II excitability for a strong positive feedback and small τ.

In the following, we study the dynamics for $a < 1$. We refer to the regimes as *excitable* (A), *oscillatory* (B), and *bistable* (C, D) according to their properties. When studying the system in the presence of noise, we concentrate on the *excitable* and the *oscillatory* regimes and study how the event-triggered feedback affects the IEI statistics.

B. Finite noise strengths

In case of finite noise strengths ($D \neq 0$) the mean IEI, of long sequences Δt_i ($N \to \infty$), in the absence of feedback is given by the mean first passage time (FPT) for the system to reach $\phi = 2\pi$ for the first time, when it was started at $\phi = 0$. For this problem, the mean FPT $\langle \Delta t_i \rangle$ is given by a well-known integral formula [37,38] and related to the mean velocity v of a Brownian particle by $\langle \Delta t_i \rangle = 2\pi/v$. Due to the periodicity of the sinus in Eq. (2), our system in the absence of feedback is equivalent to overdamped Brownian motion in a tilted periodic potential, for which the mean FPT [39,40] is given by

$$\frac{1}{r_0} = \langle \Delta t_{i,0} \rangle = \frac{\int_0^{2\pi} dx\, e^{\frac{U_0(x)}{D}} \int_{x-2\pi}^{x} dy\, e^{-\frac{U_0(y)}{D}}}{D\left(1 - e^{-\frac{2\pi\omega_0}{D}}\right)}. \tag{19}$$

Here the index 0 marks the absence of feedback. The potential $U_0(\phi)$ is given by $U_0(\phi) = -\omega_0\phi - \cos(\phi)$. For this potential, Eq. (19) can be written in terms of modified Bessel functions [41]:

$$\langle \Delta t_{i,0} \rangle = \frac{2\pi^2 \left| I_{(i\frac{\omega_0}{D})}\left(\frac{1}{D}\right)\right|^2}{D \sinh\left(\frac{\pi\omega_0}{D}\right)}. \tag{20}$$

Here $I_n(y)$ denotes the nth modified Bessel function of the first kind.

In order to account for the feedback, we use the approximation of slow varying $\Delta\omega$ (see above), which holds in the case of $\langle \Delta t_i \rangle \ll \tau$. For such τ, we can describe the effect of feedback by substituting $\omega_0 \to \omega_0 + \langle \Delta\omega \rangle$ [compare Eq. (8)] in Eq. (19). Applying this approximation to $U_0(\phi)$ leads to the extended potential $U(\phi) = -(\omega_0 + \langle \Delta\omega \rangle)\phi - \cos(\phi)$.

Since $\langle \Delta\omega \rangle$ depends on $\langle \Delta t_i \rangle$, Eq. (19) becomes self-consistent:

$$\begin{aligned}\frac{1}{r} = \langle \Delta t_i \rangle &= \frac{\int_0^{2\pi} dx\, e^{\frac{U(x)}{D}} \int_{x-2\pi}^{x} dy\, e^{\frac{-U(y)}{D}}}{D\left\{1 - \exp\left[-\frac{2\pi(\omega_0 + \langle \Delta\omega \rangle)}{D}\right]\right\}} \\ &= \frac{2\pi^2 \left| I_{(i\frac{\omega_0 + \langle \Delta\omega \rangle}{D})}\left(\frac{1}{D}\right)\right|^2}{D \sinh\left(\frac{\pi\omega_0 + \pi\langle \Delta\omega \rangle}{D}\right)}, \quad \langle \Delta t_i \rangle \ll \tau. \end{aligned} \tag{21}$$

However, for our purpose it is more advantageous to rewrite the integral in Eq. (21) as the series

$$\begin{aligned}\langle \Delta t_i \rangle = &\frac{2\pi}{\omega_0 + \langle \Delta\omega \rangle} \sum_{k=0}^{\infty} \left(\frac{1}{2D}\right)^k \\ &\times \sum_{m=0}^{k} \frac{1}{m!(k-m)!} \frac{I_{|k-2m|}\left(-\frac{1}{D}\right)}{1 + \frac{D^2(k-2m)^2}{(\omega_0 + \langle \Delta\omega \rangle)^2}}, \quad \langle \Delta t_i \rangle \ll \tau, \end{aligned} \tag{22}$$

which can be done after performing some tedious calculations, for $\omega_0 + \langle \Delta\omega \rangle \neq 0$.

Assuming a weak feedback $\langle \Delta\omega \rangle/\omega_0 \ll 1$, we can use a Taylor expansion and arrive at the implicit equation

$$\begin{aligned}\frac{1}{r} = \langle \Delta t_i \rangle \approx \langle \Delta t_{i,0} \rangle - \frac{2\pi a}{\omega_0} + \frac{4\pi^2 a}{\omega_0^2 \langle \Delta t_i \rangle} B(D,\omega_0), \\ \langle \Delta\omega \rangle \ll \omega_0, \ \langle \Delta t_i \rangle \ll \tau, \end{aligned} \tag{23}$$

for the mean FPT $\langle \Delta t_i \rangle$ in the presence of feedback.

Here $B(D,\omega_0)$ represents the series

$$\begin{aligned}B(D,\omega_0) = &\sum_{k=1}^{\infty} \left(\frac{1}{2D}\right)^k \sum_{m=0}^{k} \frac{1}{m!(k-m)!} \\ &\times \frac{I_{|k-2m|}\left(-\frac{1}{D}\right)}{1 + \frac{D^2}{\omega_0^2}(k-2m)^2} \frac{2(k-2m)^2}{\frac{\omega_0^2}{D^2} + (k-2m)^2}. \end{aligned} \tag{24}$$

If $B(D,\omega_0)$ converges, Eq. (23) has the only positive solution,

$$\begin{aligned}\langle \Delta t_i \rangle \approx \langle \Delta t_{i,0} \rangle - \frac{2\pi a}{\omega_0} + \frac{4\pi^2 a}{\omega_0^2 \langle \Delta t_{i,0} \rangle} B(D,\omega_0), \\ \langle \Delta\omega \rangle \ll \omega_0, \quad \langle \Delta t_i \rangle \ll \tau. \end{aligned} \tag{25}$$

This series is our final result for the mean FPT for large τ and weak feedback. Its evaluation compared to simulations is illustrated in Fig. 5. More details on its evaluation are given in Appendix B 1.

C. Strong noise approximation

In case of strong noise ($D \gg 1$), the first summand ($k = 0$) dominates the series [Eq. (24)] and $\langle \Delta t_i \rangle$ can be approximated by [41]

$$\frac{1}{r_0} = \langle \Delta t_{i,0} \rangle \approx \frac{2\pi}{\omega_0}, \quad D \gg 1, \tag{26}$$

in the nonfeedback case.

Since the function $B(D,\omega)$ is of order $\mathcal{O}(\frac{1}{2D})$ a similar approximation for Eq. (25) leads to

$$\begin{aligned}\langle \Delta t_i \rangle \approx \langle \Delta t_{i,0} \rangle - \frac{2\pi a}{\omega_0}, \\ D \gg 1, \quad \langle \Delta\omega \rangle \ll \omega_0, \quad \langle \Delta t_i \rangle \ll \tau, \end{aligned} \tag{27}$$

and, in combination with Eq. (26), to

$$\begin{aligned}\frac{1}{r} = \langle \Delta t_i \rangle = \frac{2\pi(1-a)}{\omega_0}, \\ D \gg 1, \quad \langle \Delta\omega \rangle \ll \omega_0, \quad \langle \Delta t_i \rangle \ll \tau. \end{aligned} \tag{28}$$

Note that this does not depend on the noise strength, as already observed by Stratonovich in the absence of feedback [41].

D. Weak noise approximation

In the excitable regime ($\omega_0 < 1$), the mean IEI in the weak noise limit can be obtained from the Kramers rate theory [43]. In the absence of feedback, the Kramers rate of generating an event

$$r_0 = \frac{\sqrt{1-\omega_0^2}}{2\pi}\, e^{-\frac{\Delta U_0}{D}}, \quad \omega_0 < 1, \quad D \ll 1. \tag{29}$$

Here $\Delta U_0 = U_{0,\max} - U_{0,\min}$ denotes the height of the potential barrier. $U_{0,\min} = -\sqrt{1-\omega_0^2} - \omega_0 \arcsin(\omega_0)$ and $U_{0,\max} = -\pi\omega_0 + \sqrt{1-\omega_0^2} + \omega_0 \arcsin(\omega_0)$ are the values of the potential at the saddle and at the SN in the absence of feedback, respectively.

If τ is large compared to the mean IEI, we can account for the feedback by substituting $\omega_0 \to \omega_0 + \langle\Delta\omega\rangle$ in Eq. (29). In the next step, we assume a weak feedback ($\Delta\omega/\omega_0 \ll 1$) and perform a Taylor expansion. The first order approximation for the potential barrier reads

$$\begin{aligned} &\Delta U = \Delta U_0 - 4\pi a r \arccos(\omega_0), \\ &\omega_0 < 1, \quad D \ll 1, \quad \langle\Delta\omega\rangle \ll \omega_0, \quad \langle\Delta t_i\rangle \ll \tau. \end{aligned} \tag{30}$$

Here ΔU denotes the barrier of the potential U mentioned above. Consequently, the barrier height becomes rate dependent and reduces for positive feedback and increases for negative feedback.

Finally, in the presence of feedback the Kramers rate [Eq. (29)] reads

$$\begin{aligned} &r = r_0 \left\{1 - 2\pi a r_0 \omega_0 \left(\frac{\omega_0}{1-\omega_0^2} - \frac{2}{D}\arccos[\omega_0]\right)\right\}, \\ &\omega_0 < 1, \quad D \ll 1, \quad \langle\Delta\omega\rangle \ll \omega_0, \quad \langle\Delta t_i\rangle \ll \tau. \end{aligned} \tag{31}$$

In the oscillatory regime we find, using the approach of Ref. [44], that the first nonzero correction to the deterministic mean IEI [Eq. (17)] is of order D^2.

E. Results obtained from simulations

Figure 5 (top) shows the analytical results in the weak noise limit [Eq. (17)], for a strong noise [Eq. (27)], as well as the series approximation [Eq. (25)] in the excitable (left) and in the oscillatory (right) regime, respectively. A double logarithmic plot of the weak noise regime in the excitable regime is shown in Appendix B. Analytical results are compared to stochastic simulations of the model [Eqs. (2) and (4)]. In the excitable regime, the approximations

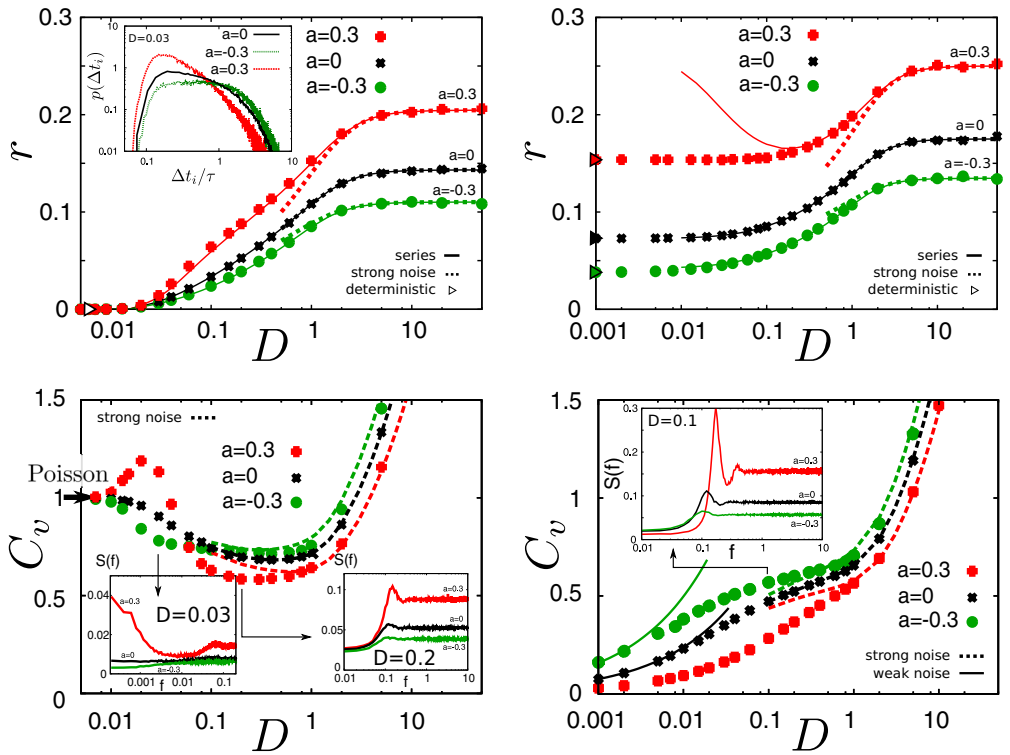

FIG. 5. (Color online) Firing rate r (top) and CV (bottom) in the excitable regime for $\omega_0 = 0.9$ (left) and the oscillatory regime for $\omega_0 = 1.1$ (right), both with $\tau = 100$. Insets show the IEI density (top left) and the power spectra (bottom) for particular noise strengths. Colors denote the particular amount of feedback. Points represent data obtained from simulations. Firing rates: (Top) Bold lines represent the series approximation Eq. (25), dashed lines show the strong noise approximation Eq. (27) (see details in Appendix B 1 for both approximations), and the triangles mark the deterministic firing rates $r = 1/\Delta t_{\text{det}}^{(1)}$ obtained from Eq. (17). Firing rates for $D < 0.02$ were calculated using the rare-event method presented in Ref. [42] and are shown in the double logarithmic plot Fig. 11 (in Appendix B 1) together with the weak noise approximation Eq. (31). CV: (Bottom) Dashed lines indicate the strong noise approximation [Eq. (37)] and bold lines (right bottom) the weak noise approximation [Eq. (40)] (see Appendix B 2 for details). In the excitable regime the weak noise limit is given by the Poisson process. Power spectra (bottom, insets) and IEI density (top left, inset) are obtained from simulations.

agree well with the simulations. Here the strong noise approximation is close to the simulation results for $D > 1$, whereas the deterministic firing rate approximates well the behavior for $D < 0.02$. Here, an even better approximation is given by the correction to the Kramers rate Eq. (31) (compare Fig. 11, Appendix B). The series approximation can be used for all D; however, strong positive feedback $a = 0.3$ produces deviations from the theoretical result and small values of D require large computation times. In the oscillatory regime we find a similar agreement, except that the series does not fit the simulations for strong positive feedback in the range of low and intermediate noise strengths. Here, the assumption of weak feedback ($\langle\Delta\omega\rangle \ll \omega_0$) does not hold anymore. Note that since $\langle\Delta\omega\rangle$ depends on the mean IEI, the series approximation leads to better results for low firing rates, i.e., in the excitable regime or for a negative feedback. In general, an increasing noise strength decreases the mean IEI, down to a constant value given by Eq. (28).

IV. EFFECT OF FEEDBACK ON OUTPUT VARIABILITY

In order to study the variability in a series of IEIs two different measures can be used. The first one is the coefficient of variation (CV),

$$C_v = \frac{\sqrt{\langle(\Delta t_i - \langle\Delta t_i\rangle)^2\rangle}}{\langle\Delta t_i\rangle}, \tag{32}$$

in which the standard deviation of the Δt_i is compared to its mean. Therefore, $C_v = 0$ corresponds to the most regular sequence and, consequently, to the most coherent one, whereas $C_v = 1$ is obtained for a completely random spike train, in which all spikes are independent of each other (Poisson process).

As a second measure of spike train regularity, one can study the power spectrum [45],

$$S(f) = \int_{-\infty}^{\infty} dt' \langle x(t)x(t+t')\rangle e^{2\pi i f t'}, \tag{33}$$

which measures the spectral components of $x(t)$. In the power spectrum, a narrow peak (possibly accompanied by more peaks at higher harmonics) indicates more coherent sequences of Δt_i.

In order to calculate the CV of Δt_i, its mean and its standard deviation $\sqrt{\langle(\Delta t_i - \langle\Delta t_i\rangle)^2\rangle}$ are needed. We first calculate the variance $\mathrm{var}(\Delta t_i)$ of Δt_i. In the absence of feedback, $\Delta\omega$ will approach zero and we can apply the formula from Ref. [40], which was derived for the variance of the FPT density in the case of Brownian motion in a tilted periodic potential,

$$\mathrm{var}(\Delta t_i) = \frac{2}{D^2\left[1-\exp\left(-\frac{2\pi\omega_0}{D}\right)\right]^3}\int_0^{2\pi} dv_1\, e^{\frac{U_0(v_1)}{D}} \times \left[\int_{v_1-2\pi}^{v_1} dv_2\, e^{\frac{-U_0(v_2)}{D}}\right]^2 \int_{v_1}^{v_1+2\pi} dy\, e^{\frac{U_0(y)}{D}}. \tag{34}$$

Here $U_0(x)$ is the potential used in the previous section. Applying several simple but tedious steps, similar to those used in the prior section, we end up with a series representation, which, after substituting $\omega_0 \to \omega_0 + \langle\Delta\omega\rangle$ and a Taylor expansion with respect to the strength of the feedback ($\langle\Delta\omega\rangle/\omega_0$), yields the first order correction to the variance,

$$\mathrm{var}(\Delta t_i) \approx \mathrm{var}(\Delta t_{i,0})\left\{1 + \frac{2\pi a}{\langle\Delta t_{i,0}\rangle} \times \left[-\frac{3}{\omega_0} + \frac{2D^2}{\mathrm{var}(\Delta t_{i,0})\omega_0^3}C(D,\omega_0)\right]\right\}, \tag{35}$$
$$\langle\Delta\omega\rangle \ll \omega_0, \quad \langle\Delta t_i\rangle \ll \tau.$$

Here $\mathrm{var}(\Delta t_{i,0})$ denotes the variance in the absence of feedback ($a = 0$) and $C(D,\omega_0)$ is a infinite series.

Strong noise approximation. Fortunately, $C(D,\omega_0)$ vanishes in the strong noise limit $D \to \infty$. Therefore, we can derive the analytical approximation for the variance,

$$\mathrm{var}(\Delta t_i) \approx \mathrm{var}(\Delta t_{i,0})\left(1 - \frac{2\pi a}{\langle\Delta t_{i,0}\rangle}\frac{3}{\omega_0}\right), \quad D \gg 1, \quad \langle\Delta\omega\rangle \ll \omega_0, \quad \langle\Delta t_i\rangle \ll \tau, \tag{36}$$

for the strong noise regime. In this regime, the variance decreases for positive and increases for negative feedback.

Using Eqs. (36) and (27), we obtain the first order correction to the CV,

$$C_v \approx C_{v,0}\left(1 - \frac{\pi a}{\omega_0\langle\Delta t_i\rangle}\right), \quad D \gg 1, \quad \langle\Delta\omega\rangle \ll \omega_0, \quad \langle\Delta t_i\rangle \ll \tau. \tag{37}$$

for the strong noise and weak feedback. Here $C_{v,0}$ denotes the CV for $a = 0$. Therefore, positive feedback decreases the CV, whereas negative feedback leads to higher variability in the strong noise regime. Comparing the strong noise approximation [Eq. (37)] to simulation [Fig. 5 (bottom)], we find that it fits the numerical results well for $D > 1$.

Weak noise approximation. In the weak noise limit, we distinguish between the excitable regime, where the IEI statistics is Poisson-like ($C_v \approx 1$), and the oscillatory regime, where the results of Ref. [44] can be applied. In the latter case, i.e., for $\omega_0 > 1$ and in the absence of feedback, the first order approximation for the variance reads

$$\mathrm{var}(\Delta t_{i,0}) \approx 2\int_0^{2\pi} d\phi \frac{D}{(\omega_0 - \sin[\phi])^3} \approx 2\pi D\frac{1+2\omega_0^2}{\left(\omega_0^2-1\right)^{5/2}}, \quad \omega_0 > 1, \quad D \ll 1. \tag{38}$$

Using this in the CV and the weak noise approximation for the mean IEI yields

$$C_{v,0} \approx \sqrt{\frac{D}{2\pi}}\sqrt{\frac{1+2\omega_0^2}{\left(\omega_0^2-1\right)^{3/2}}}, \quad \omega_0 > 1, \quad D \ll 1. \tag{39}$$

Using the substitution $\omega_0 \to \omega_0 + \langle\Delta\omega\rangle$, we can account for the feedback in case of a slow feedback time scale $\langle\Delta t_i\rangle \ll \tau$. By assuming a weak feedback $\langle\Delta\omega\rangle \ll \omega_0$, we obtain the C_v up to first order in D:

$$C_v \approx C_{v,0}\left[1 - \frac{\pi a}{\langle\Delta t_{i,0}\rangle}\frac{\omega_0^2\left(7+2\omega_0^2\right)}{\left(\omega_0^2-1\right)\left(1+2\omega_0^2\right)}\right], \quad \omega_0 > 1, \quad D \ll 1, \quad \langle\Delta\omega\rangle \ll \omega_0, \quad \langle\Delta t_i\rangle \ll \tau. \tag{40}$$

Consequently, the CV decreases for positive feedback and increases for negative feedback and hence, qualitatively, the effect of the feedback in the oscillatory regime is similar at weak and strong noise [cf. Eq. (37)].

Figure 5 (left bottom) shows the Poisson limit $C_v = 1$. However, for slightly larger D the CV varies strongly with the feedback strength. This variation is due to the dynamics of $\Delta\omega$ (see below) and cannot be described by our approach for a slow feedback time scale. In the oscillatory regime [Fig. 5 (right bottom)] the weak noise approximation [Eq. (40)] fits the data well for negative feedback and $D < 0.005$. For the positive feedback $a = 0.3$, however, the weak-feedback approximation seems to break down and, as a consequence of this, Eq. (40) produces slightly negative CVs. However, we find that for a weaker feedback with $a = 0.15$ the approximation fits the numerical results well (data not shown).

A. Excitable regime

In excitable systems increasing the noise strength does not necessarily result in higher spike train variability. Instead, there exists a minimum variability at a finite noise level. This phenomenon is known as coherence resonance (CR) and becomes apparent by a local minimum in the CV or by a pronounced peak in the power spectrum attained at an optimal value of the noise intensity. CR can occur in excitable systems due to an interplay of at least two different time scales [46,47] and has been observed in the noisy Adler's equation without feedback [3,48] and experimentally in laser systems [49,50], an electric circuit [51], a chemical reaction system [52], and electrochemical systems [53,54].

Figure 5 shows the CV (left, bottom) and the power spectrum (left bottom, inset) in the excitable regime for a slow feedback time scale $\tau = 100$. Here CR can be observed for intermediate noise strengths, where the C_v possesses a local minimum, already in the absence of feedback ($a = 0$). In the presence of negative feedback ($a < 0$), the C_v slightly increases in those regions but reduces for lower noise strengths. Consequently, it increases the region of low C_v towards lower noise strengths. Positive a, however, affects C_v in the opposite direction. Such feedback improves CR for intermediate noise levels. Note that the CV in our model in the excitable regime is always above $1/\sqrt{3} \approx 0.577$. This is similar to a quadratic IF model with noise (but without feedback) and is in marked contrast to the range of CV observed in a stochastic leaky IF model [55]; for differences in signal transmission properties of these models, see [56].

Interestingly, it also leads to an local maximum of the C_v at a low noise level ($D \approx 0.02$–0.03). Such a maximum indicates *anticoherence resonance* (ACR) [57] or *incoherence resonance* [3] and has been observed in models as a consequence of either damped subthreshold oscillations [57] or due to a finite refractory period [47]; for an experimental verification, in a laser system, see [58].

For large noise strength the behavior of the C_v can be directly understood from the analytical result Eq. (37) and is a consequence of the increased or decreased distance to the point $(\omega_0 + \langle\Delta\omega\rangle = 1)$ [47], where the system can pass the maximum of the ϕ nullcline.

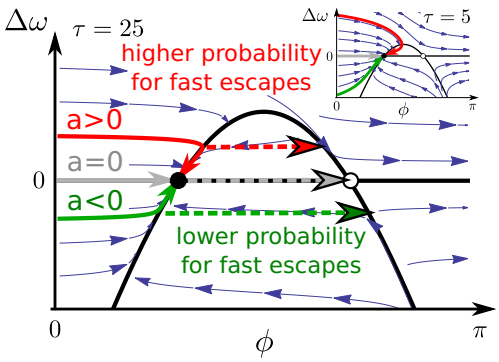

FIG. 6. (Color online) Sketch of the dynamics close to the SN for large τ and small τ (inset). Black lines represent nullclines, black dots the stable nodes, and white dots the unstable nodes, bold colored lines the deterministic trajectories, and dashed arrows the escapes from the stable branch. Thin blue arrows in the background depict the velocity field $(\dot{\phi}, \Delta\dot{\omega})$. Parameters: $\omega_0 = 0.8$, $a = 0.5, 0, -0.5$.

The behavior in the weak noise regime, however, results from the dynamics of $\Delta\omega$, which is illustrated in Fig. 6 and leads, in contrast, to the oscillatory regime, to a qualitatively different behavior of the CV in the strong and in the weak noise regime, respectively. For positive feedback, trajectory enters new cycles with positive $\Delta\omega$. Since the $\Delta\omega$ dynamics is usually slower than the ϕ dynamics, the system reaches the ϕ nullcline above the SN and then relaxes slowly toward the stable fixed point. During the relaxation, however, the system can escape the SN's basin of attraction much easier than for $\Delta\omega = 0$, because the distance to the unstable branch and the potential barrier are smaller. This leads to higher probability for small IEIs and a long tail in the FPT density [see Fig. 5 (top left, inset)], the latter resulting from the Poisson-like statistics for leaving the SN. Since the FPT density shows more probability at times much smaller than the mean IEI, the CV increases [57].

If negative feedback is applied, the trajectories enter new cycles with negative $\Delta\omega$ [see Fig. 6]. Once they reach the stable branch the probability for escapes is very low and increases when $\Delta\omega$ relaxes to zero. This reduces the FPT density [Fig. 5 (top left, inset)] for times $\Delta t < \tau$ and, consequently, reduces the CV.

Whether the feedback, finally, enhances or diminishes the CR effect depends on the interplay of both the CV modulation in the strong noise regime due to the altered distance to the point $\omega_0 + \langle\Delta\omega\rangle = 1$, described by Eq. (37), and the modulation in the weak noise regime, which is dominated by the dynamics of $\Delta\omega$, illustrated in Fig. 6. Figure 7 shows the CV for different values of τ. Note that a change in the feedback time scale τ has two effects. On the one hand, it affects the increase of $\Delta\omega$ when an event occurs $(2\pi a/\tau)$ and, on the other hand, it directly alters the time scale separation between the ϕ and the $\Delta\omega$ dynamics. Typical trajectories for a small τ are depicted in the inset in Fig. 6. Small τ enhance the modulation of the CV due to the dynamics of $\Delta\omega$ mentioned above, leading to higher CV in the weak noise (ACR) regime for $a > 0$ and to lower CV for $a < 0$. For negative feedback, the region of low C_v is shifted to higher noise strength when

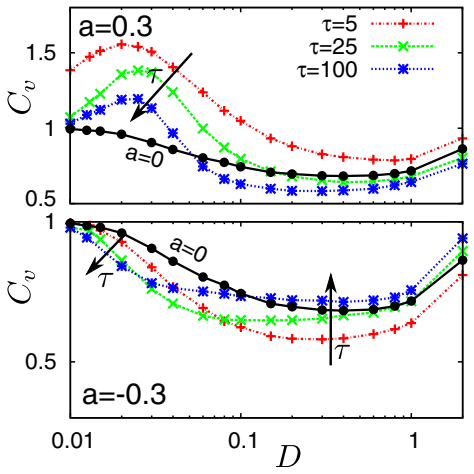

FIG. 7. (Color online) Coefficient of variation C_v plotted over the noise strength D for different values of τ obtained from simulations, for positive $a = 0.3$ (top), negative $a = -0.3$ (bottom), and without feedback $a = 0$ (black). Black arrows indicate the qualitative behavior for an increasing τ.

τ decreases. This occurs due to the larger distance to the point $\omega_0 + \langle \Delta\omega \rangle = 1$ and has been observed in Ref. [47], too.

Analyzing the power spectra, we find very different qualitative behavior in the regions of ACR and CR, respectively. For intermediate noise strength ($D = 0.2$) CR occurs [see Fig. 5 (left bottom)] and the spectrum possesses a well pronounced peak. For low frequencies $S(f \to 0)$, all simulated feedback strengths show quite similar low power. The limit of high frequencies, however, is given by the firing rate $S(f \to \infty) = r$ and, therefore, power increases for positive feedback. In the region of ACR ($D = 0.02$–0.03), the spectrum shows even more interesting behavior. Here, positive feedback leads to more power at low frequencies and increases the power in the peak. In between the spectrum possesses a minimum. Consequently, the system operates in two different frequency regimes, possessing bursting behavior. Such behavior leads to clusters of small IEIs followed by clusters of large ones.

B. Oscillatory regime

Figure 5 (right bottom) shows the CV and the power spectrum (inset) in the oscillatory regime. In this regime, the irregularity of spiking increases monotonically with the noise intensity. Interestingly, positive feedback highly reduces spike train variability for low and intermediate D. Studying the power spectrum, we find that the power at low frequencies is reduced, whereas the peak at $f \approx r$ becomes more pronounced, if positive feedback is applied.

V. FEEDBACK-INDUCED CORRELATIONS

The dynamics of $\Delta\omega$ also causes correlations of subsequent IEIs. A measure to quantify correlations of IEIs of lag n is the serial correlation coefficient (SCC) [59]

$$\rho_n = \frac{\langle (\Delta t_i - \langle \Delta t_i \rangle)(\Delta t_{i+n} - \langle \Delta t_i \rangle) \rangle}{\mathrm{var}(\Delta t_i)}. \tag{41}$$

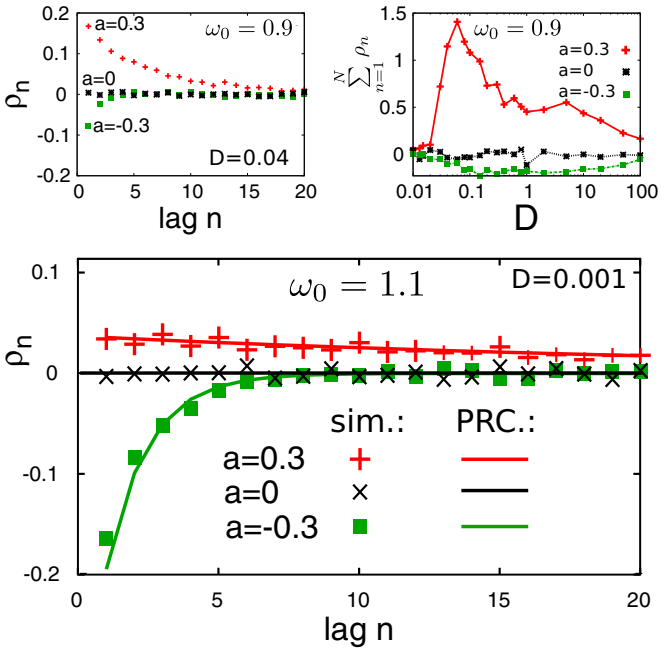

FIG. 8. (Color online) SCC over several lags (top left) for $D = 0.04$, the sum of the first $N = 100$ SCCs plotted over noise strength (top right) in the excitable regime ($\omega_0 = 0.9$) (top) and SCC over several lags in the oscillatory regime ($\omega_0 = 1.1$) (bottom). Excitable regime (top): All results are obtained from simulation. Oscillatory regime (bottom): Numerical results (sim.) are shown together with the analytical approximation [Eq. (43)]. Parameter: $\tau = 100$.

If correlations are positive ($\rho_n > 0$), longer Δt_i are, on average, followed by longer Δt_{i+n} (and/or shorter Δt_i by shorter Δt_{i+n}). Negative correlations between adjacent intervals ($\rho_1 < 0$) could be caused by an alternation between short and long intervals. The low-frequency limit of the power spectrum is also connected to the SCCs. It holds [59]

$$\lim_{f \to 0} S(f) = r C_v^2 \left(1 + 2 \sum_{k=1}^{\infty} \rho_k \right). \tag{42}$$

Consequently, cumulative IEI correlations can be also studied using the power spectrum.

A. Numerical results in the excitable regime

In the excitable regime, the dynamics of $\Delta\omega$ not only leads to ACR in the weak noise regime, but also causes serial correlations. The SCC of several lags is depicted in Fig. 8 (top left). It shows strong, slowly decaying positive and strong, fast-decaying negative correlations for a noise strength of $D = 0.04$, close to the value at which the ACR is observed for positive feedback [compare Fig. 5 (left bottom)]. This can be understood by studying the trajectories depicted in Fig. 6. If positive feedback ($a > 0$) is applied, fast escapes from the SN, on average, will lead to higher $\Delta\omega$ at $\phi = 2\pi$ (compare Fig. 6). Consequently, $\Delta\omega$ will be higher in subsequent IEIs, which increases the probability for fast escapes (small Δt_i), and, therefore, causes positive IEI correlations. However, for negative feedback, the opposite behavior occurs. Here a fast escape (short Δt_i) leads, on

average, to lower $\Delta\omega$ for subsequent cycles and, therefore, further reduces the probability for short Δt_{i+n}, which leads to negative IEI correlations.

Analyzing the sum of the first N SCCs [Fig. 8 (top right)], we find that correlations possess a maximum in the regime of ACR. This can be understood as follows: If D is small, the mean IEI is larger than the feedback time scale τ; therefore, perturbations of $\Delta\omega$ are already relaxed when the system can escape the SN, leading to less correlated IEIs. However, if D is large, noise dominates the dynamics and leads to less correlations in the sequence, too. Close to the local maximum of the C_v, however, we find strong positive (for $a > 0$) and strong negative (for $a < 0$) serial correlations. Combining these findings with Eq. (42) and using that C_v is of order 1, we find that the increase in the power at low frequencies [see Fig. 5 (left bottom, inset)] reflects these correlations.

B. Approximation for a slow feedback time scale in the oscillatory regime

If the system evolves on a LC, the SCC in the weak noise limit can be expressed by a product of the form

$$\rho_n = (\eta V)^{n-1}\rho_1, \quad n \geqslant 1, \quad \omega_0 > 1, \quad D \ll 1. \tag{43}$$

This result was derived for the perfect IF neuron [16] and for a general IF neuron [30], both subjected to an adaptation current (negative feedback), respectively. It can be generalized to positive feedback as long as a LC exists.

The first correlation coefficient ρ_1 is given by

$$\rho_1 = -\eta(1-V)\frac{1-\eta^2 V}{1+\eta^2-2\eta^2 V}. \tag{44}$$

Here η is determined by the deterministic IEI Δt_{det} [Eq. (17)],

$$\eta = \exp\left(-\frac{\Delta t_{\text{det}}}{\tau}\right), \tag{45}$$

and the term V reads

$$V = 1 - \frac{\Delta\omega_{lc} + \frac{2\pi a}{\tau}}{\tau}\Theta, \tag{46}$$

where Θ is accessible by the phase response curve (PRC) $Z(t)$ [30]

$$\Theta = -\int_0^{\Delta t_{\text{det}}} dt\; Z(t)e^{-\frac{t}{\tau}}. \tag{47}$$

These formulas have been developed for a perfect [16] or general multidimensional IF models [30] with a spike-triggered linear dynamics for a negative feedback. We have verified that the approach of Ref. [30] also applies to the case of positive feedback as long as a steady state exists, i.e., for $a < 1$.

For our system, the PRC can be approximated for a slow feedback time scale ($\Delta t_{\text{det}} \ll \tau$) (see Appendix C). In this limit, Θ reads

$$\Theta = -\left(1-e^{-\frac{\Delta t_{\text{det}}}{\tau}}\right)\frac{\tau}{(\omega_0+\Delta\omega_{lc})} \times \frac{1+\tau+\tau^2(\omega_0+\langle\Delta\omega\rangle)^2}{1+\tau^2[(\omega_0+\langle\Delta\omega\rangle)^2-1]}, \tag{48}$$

$\Delta t_{\text{det}} \ll \tau.$

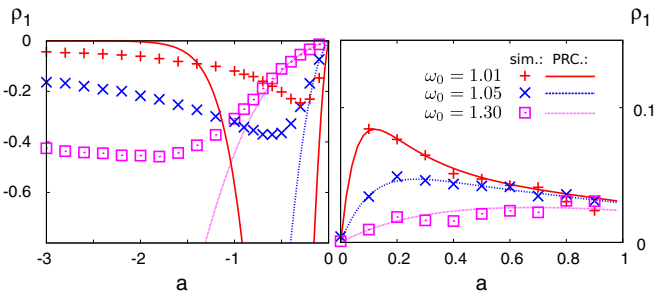

FIG. 9. (Color online) Influence of the distance to the bifurcation on the SCC at lag 1 for $a < 0$ (left) and $a > 0$ (right). The theory Eq. (43) (lines) is compared to simulations for a very low noise level $D = 0.001$ (points). Close to the bifurcation ($\omega = 1.01$), ρ_1 behaves nonmonotonically, possessing a local minimum for negative feedback and a local maximum for positive feedback, respectively. If the distance to the bifurcation is increased ($\omega = 1.05$, $\omega = 1.3$), the local minimum moves to stronger negative feedback. For positive feedback, however, the local maximum vanishes in a large distance to the bifurcation. Consider the difference of the total range of a and ρ_1 in the two panels. Parameters: $\tau = 100$.

Here, Θ is always negative and η is close, but smaller than one. Consequently, V is larger than one for $a > 0$ and smaller than one for $a < 0$. This causes ρ_1 to have the same sign as a [compare Eq. (44) for $\eta \lesssim 1$].

C. Comparison of theory and numerical results in the oscillatory regime

1. Distance to the bifurcation

Figure 9 shows the analytical results Eq. (44) for ρ_1 compared to those obtained from simulations for different distances to the saddle-node bifurcation at $\omega_0 = 1$. Interestingly, maximal positive correlations (for $a > 0$) become stronger, whereas maximal negative correlations (for $a < 0$) become weaker by approaching the bifurcation. Note that close to the bifurcation or for strong negative feedback, Δt_{det} becomes comparable to τ [see Fig. (3)] and the assumption of a slow feedback time scale ($\Delta t_{\text{det}} \ll \tau$) does not hold anymore. For this reason the approximation fails quantitatively for large negative values of a.

2. Nonmonotonic behavior

Another interesting observation can be made in Fig. 9: Stronger feedback does not necessarily increase ρ_1. Instead, the SCC at lag 1 possesses a minimum for negative feedback and a maximum when positive feedback is applied. The maximum for positive feedback, however, vanishes if the distance to the bifurcation is increased.

In order to understand how stronger feedback can lead to smaller ρ_1, it is helpful to consider the particular trajectories, shown in Fig. 2 (center). Suppose that the system evolves on the LC and highly negative feedback is applied. In that case, its trajectory looks like the lower one in Fig. 2 (center). Such trajectories spend the main part of the IEI close to the stable branch of the ϕ nullcline. The system slowly evolves along the ϕ nullcline until $\omega_0 + \Delta\omega > 1$. Close to the bifurcation

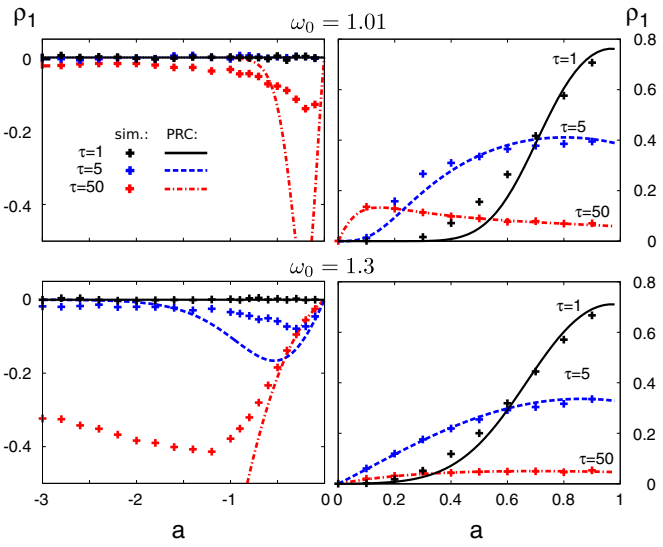

FIG. 10. (Color online) Influence of τ on the SCC at lag 1 in the weak noise limit for $a < 0$ (left) and $a > 0$ (right) obtained from Eq. (43) using Eq. (C5) for Θ (PRC) and from simulations (sim) using $D = 0.001$. Close to the bifurcation (top), decreasing τ shifts the maximum of ρ_1 to higher a. Due to the reduced feedback time scale, subsequent IEIs become more uncorrelated if weak feedback is applied. However, for $a \to 1$ the mean IEI runs to zero and becomes comparable to τ, even with small τ. For negative feedback, small τ highly reduce ρ_1.

($\omega_0 \gtrsim 0$), however, this requires $\Delta\omega$ to approach small values. Consequently, information on perturbations, for instance, due to prior longer (or shorter) IEIs is reduced, which decreases ρ_1 for strong negative feedback. In the case of positive or weak negative feedback this effect acts in the opposing direction, since $\Delta\omega$ does not have to increase to pass the maximum of the ϕ nullcline. Here slightly higher $\Delta\omega(t_i)$ lead to disproportional shorter IEIs Δt_{i+1}, whereas initially slightly lower $\Delta\omega(t_i)$ lead to much longer Δt_{i+1}, if the system is close to the bifurcation point. Consequently, strong positive correlation between subsequent lags occurs. However, for highly positive feedback, the LC is far from the ϕ nullcline (see Fig. 2, center). Here these nonlinear effects disappear and ρ_1 decreases again.

3. *Influence of the feedback time scale*

In Fig. 10, we show ρ_1 as a function of the feedback strength for different τ. Here, interestingly, smaller τ may lead to stronger correlations for $a > 0$, whereas ρ_1 decreases for $a < 0$. This occurs due to the increased distance to the ϕ nullcline, which leads to smaller IEIs for positive feedback. Since the mean IEI runs to zero for $a \to 1$, these correlations are present for strong positive feedback, even for very small τ. However, negative feedback leads to larger IEIs, so that perturbations of $\Delta\omega$ cannot survive.

VI. SUMMARY AND DISCUSSION

We have studied the effect of event-triggered feedback on the dynamics and output statistics of a noise-driven phase oscillator.

Analytical results for the mean IEIs were derived, which show besides the emergence of a bistable regime, that positive feedback leads to a change the bifurcation structure of the system and the excitability class. Investigating the influence of the feedback on the output statistics in the excitable regime, we observed that whereas CR can be observed even without any feedback, only positive feedback leads to ACR at low noise strengths.

For both kinds of feedback, we found serial correlations in the sequence of IEIs, which can be approximated analytically in the oscillatory regime for a weak noise and a large time scale separation between the phase and the feedback dynamics, which can be found in cases of spike-triggered feedback due to slow inhibitory currents or slow decaying variations in external ion concentrations in neural systems. Close to the bifurcation from the excitable to the oscillatory regime, we find a nonmonotonic behavior of the correlation between adjacent IEIs and the feedback strength, which indicates that maximal correlations occur at an optimal feedback strength.

Our general approach can be used to understand the role of individual slow processes on the IEI statistics in neurons, excitable lasers, or other pulse-generating systems that operate close to a SNIC bifurcation (class I excitability) or to identify the source of serial correlations in the IEI sequence. Our results illustrate that event-triggered feedback can be used to reduce (or increase) the output variability. This is particularly interesting in information processing systems, in which this variability is the limiting factor for a reliable signal transmission.

ACKNOWLEDGMENTS

This paper was developed within the scope of IRTG 1740/TRP 2011/50151-0, funded by the DFG/FAPESP and by the BMBF (Grant No. FKZ:01GQ1001A).

APPENDIX A: SIMULATION TECHNIQUES

All simulations were performed, using the Euler method for the numerical integration of the system Eqs. (2) and (4). The integration time step was chosen to be 10^{-4} for $D < 1$ and 10^{-6} for larger D. After an equilibration time of 100τ, IEIs were recorded up to an ensemble of 10^5 IEIs. From this series of Δt_i, the mean firing rate, the CV, the power spectrum, and the SCC were calculated.

In the excitable regime, the firing rate becomes very low, especially for low noise levels. For such weak noise ($D < 0.02$), we used the rare-event method presented in Ref. [42]. Here the parameters, named according to the notation in the reference, read as follows: borders of the simulated area, $L_\phi^- = -\pi/2$, $L_\phi^- = -2\pi$, $L_\omega^- = -\omega_0$, $L_\omega^+ = 1.5$; walkers per box, $N = 2$; size of a time step, $h = 0.1$; box size in ϕ direction, $\Delta\phi_{\text{box}} = 0.1\sqrt{2Dh}$; box size in $\Delta\omega$ direction, $\Delta\omega_{\text{box}} = 1/(2\tau)$. Simulations were performed for a time $T_{\text{sim}} = 20\,000$. After entering the stationary regime, the probability current through the absorbing boundary at $\phi = 2\pi$ was recorded and, finally, averaged to get the mean firing rate.

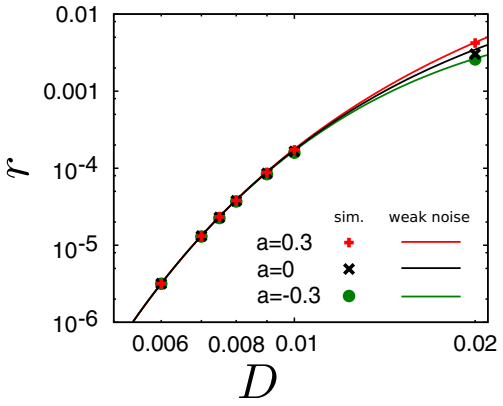

FIG. 11. (Color online) The firing rate in the excitable regime obtained from simulations (points) for a weak noise compared to the analytic approximation [Eq. (31)] (lines). Note the double logarithmic scale. Simulations for $D \leqslant 0.01$ were performed using the rare-event method presented in Ref. [42]. Parameters: $\omega_0 = 0.9$, $\tau = 100$.

APPENDIX B: DETAILS OF FIG. 5

1. Firing rates

The series approximation was calculated by using Eq. (25). For $B(D,\omega_0)$ the terms ($k = 1,2,\ldots,500$) were evaluated with high numerical precision. $\langle \Delta t_{i,0} \rangle$ was obtained from Eq. (20). For large D fewer terms are needed to approximate the firing rate well. However, for $D \approx 0.01$ a few hundred terms are needed and must be calculated with high precision. For even smaller values of D the computation time becomes too large. Therefore, the series approximation in Fig. 5 (top) is shown for $D \geqslant 0.01$.

The strong noise approximation is given by Eq. (27). Here $\langle \Delta t_{i,0} \rangle$ was obtained from Eq. (20), too.

The weak noise approximation [Eq. (31)] was evaluated using Eq. (29) for r_0 and is illustrated in Fig. 11 together with results from simulations.

2. Coefficient of variation

The strong noise approximation was calculated from Eq. (37), where Eqs. (20), (34), and (32) were used for $\langle \Delta t_{i,0} \rangle$ and $C_{v,0}$.

The weak noise approximation in the oscillatory regime was obtained from Eq. (40), where Eqs. (20) and (39) were used for $\langle \Delta t_{i,0} \rangle$ and $C_{v,0}$.

APPENDIX C: CALCULATION OF Θ USING THE PHASE RESPONSE CURVE

We can calculate Θ, using Eq. (47), i.e., by calculating the PRC. In our case the PRC is given by [30]

$$Z(t) = Z_{\mathrm{ev}}(\Delta t_{\mathrm{det}}) \exp\left\{-\int_t^{\Delta t_{\mathrm{det}}} dt' \cos[\phi_{lc}(t')]\right\}. \quad \text{(C1)}$$

Here $Z_{\mathrm{ev}}(\Delta t_{\mathrm{det}}) = 1/(\omega_0 + \Delta\omega_{lc})$ is the inverse ϕ velocity when an event occurs, if the system evolves on the deterministic LC and $\phi_{lc}(t)$ is the corresponding ϕ solution.

In order to calculate the PRC, we first solve Eq. (C1) for the nonfeedback case and account for feedback by substituting $\omega_0 \to \omega_0 + \langle \Delta\omega \rangle$ afterwards. In the nonfeedback case, $\phi_{lc}(t)$ can be obtained by integrating Eq. (1), considering $\phi_{lc}(0) = 0$ and the smoothness of $\phi_{lc}(t)$ in the interval $t \in [0, \Delta t_{\mathrm{det}}]$. This yields

$$\phi_{lc}(t) \backsimeq 2 \arctan\left(\frac{1}{\omega_0}\left\{1 - \Omega_0 \tan\left[\arctan\left(\frac{1}{\Omega_0}\right) - \frac{\Omega_0}{2} t\right]\right\}\right). \quad \text{(C2)}$$

Here $\Omega_0 := \sqrt{\omega_0^2 - 1}$ and $\backsimeq$ denotes equality modulo 2π. Putting $\phi_{lc}(t)$ into Eq. (C1), the PRC in the nonfeedback case can be calculated. After some tedious steps, we get

$$Z(t) = Z_{\mathrm{ev}}(\Delta t_{\mathrm{det}})\left[1 + \frac{1 + \Omega_0 \sin(\Omega_0 t) - \cos(\Omega_0 t)}{\Omega_0^2}\right]. \quad \text{(C3)}$$

The result for Θ can be obtained from Eq. (47). This yields

$$\Theta = -\left(1 - e^{\frac{-\Delta t_{\mathrm{det}}}{\tau}}\right) Z_{\mathrm{ev}}(\Delta t_{\mathrm{det}}) \tau \frac{1 + \tau + \tau^2 \omega_0^2}{1 + \tau^2(\omega_0^2 - 1)}. \quad \text{(C4)}$$

Finally, we account for the feedback by substituting $\omega_0 \to \omega_0 + \langle \Delta\omega \rangle$, which yields

$$\Theta = -\left(1 - e^{\frac{-\Delta t_{\mathrm{det}}}{\tau}}\right) \frac{\tau}{(\omega_0 + \Delta\omega_{lc})} \frac{1 + \tau + \tau^2(\omega_0 + \langle \Delta\omega \rangle)^2}{1 + \tau^2[(\omega_0 + \langle \Delta\omega \rangle)^2 - 1]}, \quad \tau \gg \Delta t_{\mathrm{det}}. \quad \text{(C5)}$$

Expanding this for large $\tau \gg 1$, the zeroth order term reads

$$\Theta \approx -\frac{\Delta t_{\mathrm{det}}(\omega_0 + \langle \Delta\omega \rangle)}{(\omega_0 + \langle \Delta\omega \rangle)^2 - 1}, \quad \tau \gg \Delta t_{\mathrm{det}}. \quad \text{(C6)}$$

[1] G. B. Ermentrout and J. Rinzel, Am. J. Physiol. **246**, R102 (1984).
[2] Y. Kuramoto, *Chemical Oscillations, Waves, and Turbulence* (Springer-Verlag, Tokyo, 1984).
[3] B. Lindner, J. Garcıa-Ojalvo, A. Neiman, and L. Schimansky-Geier, Phys. Rep. **392**, 321 (2004).
[4] R. Adler, Proc. IRE **34**, 351 (1946).
[5] M. Giudici, C. Green, G. Giacomelli, U. Nespolo, and J. R. Tredicce, Phys. Rev. E **55**, 6414 (1997).
[6] D. Goulding, S. P. Hegarty, O. Rasskazov, S. Melnik, M. Hartnett, G. Greene, J. G. McInerney, D. Rachinskii, and G. Huyet, Phys. Rev. Lett. **98**, 153903 (2007).
[7] E. M. Izhikevich, *Dynamical Systems in Neuroscience: The Geometry of Excitability and Bursting* (MIT, Cambridge, MA, 2007).
[8] W. Stewart, Appl. Phys. Lett. **12**, 277 (1968).
[9] S. H. Strogatz, *Nonlinear Dynamics and Chaos: With Applications to Physics, Biology, Chemistry, and Engineering* (Addison-Wesley, Reading, MA, 1994).
[10] R. Aust, P. Hövel, J. Hizanidis, and E. Schöll, Eur. J. Phys. Spec. Top. **187**, 77 (2010).
[11] N. Fourcaud and N. Brunel, Neural Comput. **14**, 2057 (2002).
[12] A. N. Burkitt, Biol. Cybern. **95**, 1 (2006).
[13] Y. H. Liu and X. J. Wang, J. Comput. Neurosci. **10**, 25 (2001).

[14] J. Benda and A. V. Herz, Neural Comput. **15**, 2523 (2003).
[15] M. J. Chacron, B. Lindner, L. Maler, A. Longtin, and J. Bastian, Proc. SPIE **5841**, 150 (2005).
[16] T. Schwalger, K. Fisch, J. Benda, and B. Lindner, PLoS Comput. Biol. **6**, e1001026 (2010).
[17] O. Avila-Akerberg and M. J. Chacron, Exp. Brain Res. **210**, 353 (2011).
[18] U. Strauss, F. Zhou, J. Henning, A. Battefeld, A. Wree, R. Köhling, S. Haas, R. Benecke, A. Rolfs, and U. Gimsa, J. Neurophysiol. **99**, 2902 (2008).
[19] D. E. Postnov, F. Müller, R. B. Schuppner, and L. Schimansky-Geier, Phys. Rev. E **80**, 031921 (2009).
[20] F. Fröhlich, M. Bazhenov, V. Iragui-Madoz, and T. J. Sejnowski, Neuroscientist **14**, 422 (2008).
[21] F. Fröhlich, M. Bazhenov, I. Timofeev, M. Steriade, and T. Sejnowski, J. Neurosci. **26**, 6153 (2006).
[22] D. J. Derickson, R. J. Helkey, A. Mar, P. A. Morton, and J. E. Bowers, Appl. Phys. Lett. **56**, 7 (1990).
[23] T. Schwalger, J. Tiana-Alsina, M. Torrent, J. Garcia-Ojalvo, and B. Lindner, Eur. Phys. Lett. **99**, 10004 (2012).
[24] E. M. Ozbudak, M. Thattai, H. N. Lim, B. I. Shraiman, and A. Van Oudenaarden, Nature (London) **427**, 737 (2004).
[25] P. J. Choi, L. Cai, K. Frieda, and X. S. Xie, Science **322**, 442 (2008).
[26] B. Ermentrout, Neural Comput. **10**, 1721 (1998).
[27] E. Urdapilleta, Phys. Rev. E **83**, 021102 (2011).
[28] T. Schwalger, D. Miklody, and B. Lindner, Eur. Phys. J. Spec. Top. **222**, 2655 (2013).
[29] E. Urdapilleta, Phys. Rev. E **84**, 041904 (2011).
[30] T. Schwalger and B. Lindner, Front. Comput. Neurosci. **7**, 164 (2013).
[31] M. J. Chacron, B. Lindner, and A. Longtin, Phys. Rev. Lett. **92**, 080601 (2004).
[32] M. Chacron, B. Lindner, and A. Longtin, J. Comput. Neurosci. **23**, 301 (2007).
[33] M. J. Chacron, A. Longtin, M. St-Hilaire, and L. Maler, Phys. Rev. Lett. **85**, 1576 (2000).
[34] S. A. Prescott and T. J. Sejnowski, J. Neurosci. **28**, 13649 (2008).
[35] F. Farkhooi, M. F. Strube-Bloss, and M. P. Nawrot, Phys. Rev. E **79**, 021905 (2009).
[36] S. Shinomoto and Y. Kuramoto, Prog. Theor. Phys. **75**, 1105 (1986).
[37] A. J. Siegert, Phys. Rev. **81**, 617 (1951).
[38] V. S. Anishchenko, V. Astakhov, A. Neiman, T. Vadivasova, and L. Schimansky-Geier, *Nonlinear Dynamics of Chaotic and Stochastic Systems: Tutorial and Modern Developments* (Springer, Berlin, Heidelberg, 2007).
[39] H. Risken, *The Fokker-Planck Equation* (Springer, Berlin, 1984).
[40] P. Reimann, C. Van den Broeck, H. Linke, P. Hänggi, J. M. Rubi, and A. Pérez-Madrid, Phys. Rev. E **65**, 031104 (2002).
[41] R. L. Stratonovich, *Topics in the Theory of Random Noise* (Gordon & Breach, New York, 1967), Vol. 2.
[42] J. A. Kromer, L. Schimansky-Geier, and R. Toral, Phys. Rev. E **87**, 063311 (2013).
[43] P. Hänggi, P. Talkner, and M. Borkovec, Rev. Mod. Phys. **62**, 251 (1990).
[44] F. T. Arecchi and A. Politi, Phys. Rev. Lett. **45**, 1219 (1980).
[45] K. Pakdaman, S. Tanabe, and T. Shimokawa, Neural Networks **14**, 895 (2001).
[46] A. S. Pikovsky and J. Kurths, Phys. Rev. Lett. **78**, 775 (1997).
[47] B. Lindner, L. Schimansky-Geier, and A. Longtin, Phys. Rev. E **66**, 031916 (2002).
[48] M. Qian, G.-X. Wang, and X.-J. Zhang, Phys. Rev. E **62**, 6469 (2000).
[49] G. Giacomelli, M. Giudici, S. Balle, and J. R. Tredicce, Phys. Rev. Lett. **84**, 3298 (2000).
[50] O. V. Ushakov, H.-J. Wünsche, F. Henneberger, I. A. Khovanov, L. Schimansky-Geier, and M. A. Zaks, Phys. Rev. Lett. **95**, 123903 (2005).
[51] D. E. Postnov, S. K. Han, T. G. Yim, and O. V. Sosnovtseva, Phys. Rev. E **59**, R3791 (1999).
[52] K. Miyakawa and H. Isikawa, Phys. Rev. E **66**, 046204 (2002).
[53] I. Z. Kiss, J. L. Hudson, G. J. Escalera Santos, and P. Parmananda, Phys. Rev. E **67**, 035201 (2003).
[54] G. J. Escalera Santos, M. Rivera, and P. Parmananda, Phys. Rev. Lett. **92**, 230601 (2004).
[55] R. D. Vilela and B. Lindner, J. Theor. Biol. **257**, 90 (2009).
[56] R. D. Vilela and B. Lindner, Phys. Rev. E **80**, 031909 (2009).
[57] A. M. Lacasta, F. Sagués, and J. M. Sancho, Phys. Rev. E **66**, 045105 (2002).
[58] S. Sergeyev, K. O'Mahoney, S. Popov, and A. T. Friberg, Opt. Lett. **35**, 3736 (2010).
[59] D. Cox and P. Lewis, *The Statistical Analysis of Series of Events* (Wiley & Sons, New York, 1966).